Advancing Structural Battery Composites: Robust Manufacturing for Enhanced and Consistent Multifunctional Performance

(article starts on next page)

RESEARCH ARTICLE

ADVANCED
ENERGY & SUSTAINABILITY
RESEARCH
Open Access

www.advenergysustres.com

Advancing Structural Battery Composites: Robust Manufacturing for Enhanced and Consistent Multifunctional Performance

Mohammad Siam Siraj, Samia Tasneem, David Carlstedt, Shanghong Duan, Marcus Johansen, Carl Larsson, Johanna Xu, Fang Liu, Fredrik Edgren, and Leif E. Asp*

Multifunctional materials offer a possibility to create lighter and more resource-efficient products and thereby improve energy efficiency. Structural battery composites are one type of such a multifunctional material with potential to offer massless energy storage for electric vehicles and aircraft. Although such materials have been demonstrated, their performance level and consistency must be improved. Also, the cell dimensions need to be increased. Herein, a robust manufacturing procedure is developed and structural battery composite cells are repeatedly manufactured with double the multifunctional performance and size compared to state-of-the-art structural battery cells. Furthermore, six structural battery cells are selected and laminated into a structural battery composite multicell demonstrator to showcase the technology. The multicell demonstrator performance is characterized for two different electrical configurations. The low variability in the multifunctional properties of the cells verifies the potential for upscaling offered by the proposed manufacture technique.

1. Introduction

E-mobility across transport modes is currently being developed to mitigate climate change, eliminating impact on the climate from emission of greenhouse gases from all types of vehicles. Ambitious targets to achieve climate neutrality can be found on all continents. For example, in July 2021, the European Commission released its "Fit for 55" legislation package, which contains important guidelines for the future of the automotive industry: All new cars sold in the EU must be zero-emission vehicles from 2035.[1] To realize electric vehicles, electrical energy stored in lithium-ion (Li-ion) batteries is a key technology, complemented by other alternative such as fuel cells. In the automotive sector, Li-ion batteries are currently the preferred solution for energy storage. The electric vehicles have large battery packs to meet customers' request for long driving range and therefore become excessively heavy and expensive. For instance, roughly 25% of the mass of the Tesla Model S (85 kWh version) comes from the battery pack.[2] Thus, current battery electric vehicle solutions are not very energy efficient. This study addresses a multifunctional material aimed to increase energy efficiency of electric road vehicles, boats, and ships as well as aircraft, providing intrinsic energy-storage capabilities in the vehicle interior and exterior structures. By combining several functions into one material, it is possible to create lighter and more resource-efficient products and thereby improve energy efficiency and usability.[3] In this way, customers' drive range anxiety can be relieved and energy consumption in transportation significantly reduced.[2,4] Composite materials that can carry mechanical loads while storing electrical energy have been coined as structural batteries.[5–8] Potentially, structural batteries can provide massless energy storage in future electric vehicles.

Current state-of-the-art structural battery composites are made from carbon fibers.[5,9] The composite has a laminated architecture, very similar to traditional composites and conventional Li-ion batteries. The idea is for every material constituent to play, at least, dual roles in the composite material. For example, in the negative electrode (anode), the carbon fiber is the active electrode material, i.e., host for lithium, conducts electrons as current collector, and carries mechanical load as reinforcement.[10] A carbon fiber–based positive electrode (the cathode) is under development, where the carbon fibers are coated with lithium iron phosphate (LFP) particles.[11,12] In this design, the carbon fiber

M. S. Siraj, S. Tasneem, S. Duan, M. Johansen, C. Larsson, J. Xu, F. Liu, L. E. Asp
Department of Industrial and Materials Science
Chalmers University of Technology
SE-412 96 Gothenburg, Sweden
E-mail: leif.asp@chalmers.se

D. Carlstedt
Department of Aeronautics and Astronautics
Stanford University
Stanford, CA 94305, USA

F. Edgren
Body Technology
Volvo Cars
405 31 Gothenburg, Sweden

The ORCID identification number(s) for the author(s) of this article can be found under https://doi.org/10.1002/aesr.202300109.

**ADVANCED
SCIENCE NEWS**

www.advancedsciencenews.com

**ADVANCED
ENERGY & SUSTAINABILITY
RESEARCH**
Open Access

www.advenergysustres.com

has the role as electron conductor, reinforcement, and scaffold for the LFP coating. It should be noted that a structural battery utilizing both a carbon fiber–based positive and negative electrode is still to be demonstrated. State-of-the-art structural battery cells instead use a commercial LFP-coated aluminum foil as the positive electrode.[5,9] The two electrodes are separated by a glass fiber separator and the stack is impregnated with a structural battery electrolyte (SBE).[13,14] The SBE is a multifunctional composite matrix material with the tasks to transfer mechanical loads between fibers as well as between layers, i.e., plies of fibers, and to transport lithium ions, i.e., be ionically conductive. The utilized SBE is a bi-continuous multiphase material. Mechanical performance is provided by a porous glassy polymer. Ionic conductivity is achieved as the pore volume in the glassy polymer is occupied by an ionically conductive solution.[15]

The first-generation structural battery composite cells were synthesized inside a glove box, using a highly manual procedure. The electrodes were cut and stacked on each side of a separator in a partially welded pouch bag and the SBE mixture was applied via a pipette, as described by Asp et al.[5] The remaining sides of the bag were then sealed under vacuum and the sealed pouch bag was taken out of the glove box and transferred into an oven and cured at elevated temperature. The manual procedure caused several problems and does not offer any option for upscaling and industrialization. First, the number of electrochemically dead cells after curing was high. This can be explained that by any single astray fiber may cause the cell to short circuit. Second, the variation in electrochemical capacity and elastic modulus was high. This poses problems, particularly for multicell devices.[9] Large differences in capacity and impedance between cells must be avoided as system performance will be governed by the properties of the weakest cell. The large variation in properties between cells observed by Xu et al. was partly due to problems with precise positioning of the electrodes during the stacking of layers in the manual operation inside the glove box.[9] Finally, larger cells were difficult to make with the developed technique, as handling and positioning of larger electrodes were difficult.

In this article, we adapt a resin-infusion technique developed for structural negative half-cells and shape morphing actuator and sensor composites for the manufacture of structural battery composite full cells.[16–18] In the technique developed by Zenkert and co-workers, the carbon fiber electrode is impregnated with the SBE using an ordinary vacuum-infusion technique to form a unidirectional lamina with good multifunctional performance. This was done using the same spread tow (Toray T800S) fibers utilized in the structural battery full cells investigated here. The developed technique allows for cell preparation and resin infusion to be performed outside the glove box in ambient conditions, as illustrated in **Figure 1**, significantly increasing precision in the layup operation. The quality of the manufacturing process is evaluated by the performance and consistency of the manufactured cells. Finally, a structural battery composite multicell laminate with six cells is demonstrated for different electrical configurations. The experience gained working on a multicell device will prepare us for design and manufacture of more sophisticated demonstrators as those showcased for structural supercapacitors, using multiple packs of stacked cells in automotive and aeronautical applications.[19]

2. Results and Discussion

2.1. Electrochemical Performance

The specific capacities and energy densities of the tested structural battery cells are presented in **Table 1**. Both cell types tested had a nominal voltage during discharge of 2.7 V. Typical charge/discharge voltage profiles for a Whatman glass microfiber filters, Grade GF/A (Whatman GF/A) separator cell at two C-rates are provided in Figure S1, Supporting Information. All tested battery cells showed similar electrochemical performance. In Table 1, the energy densities measured at approximately 0.05C (i.e., a discharge time of 20 h) of the battery cells are presented. The reported energy densities are based on the total mass of the battery cell (i.e., accounting for the mass of the electrodes, separator, SBE, and current collectors in the cell). The energy density for the cells with Whatman GF/A and GF plain weave separator are 27.5 and 41.2 Wh kg^{-1}, respectively. These energy densities show exceptional improvement toward the theoretical maximum energy densities for the two cell designs reported by Asp et al.[5] That is, the energy density of the Whatman GF/A cell is 73% of its calculated maximum energy density of 37.7 Wh kg^{-1}, and the measured energy density of the GF plain weave cell is 68% of its theoretical maximum value of 60.6 Wh kg^{-1}. The separators used are significantly thicker than separators used in conventional Li-ion batteries. They here serve as model material and needs to be replaced with thinner ones in the future to improve energy and power densities of the cells. Here, the thinner GF plain weave separator results in a higher volumetric energy density for the structural battery cell, since cell thickness is greatly reduced. Also, the gravimetric energy density is increased as the amount of separator material and SBE is reduced.

In Table 1, electrochemical performance metrics for the first-generation structural batteries are reported for comparison.[5] It can be noted that the specific capacity and the energy density of the cells manufactured via resin infusion are more than double that of previous reported data. In contrast, only moderate improvements in power density are found. It should be noted that the specific power reported here is calculated for tests at 1C, whereas it was measured at 3C in the previous study. The specific power for the two cell types at 1C are 8.5 and 12.4 W kg^{-1}, for the Whatman GF/A and GF plain weave separator cells, respectively.

The electrochemical performance of a structural battery composite with a Whatman GF/A separator is presented in **Figure 2**. Figure 2a shows the energy density for a cell at different true C-rates. A moderate capacity fade is identified, indicating reasonably stable energy densities at the studied C-rates. In Figure 2b, capacity retention of a structural battery cell with a Whatman GF/A separator over 500 cycles at approximately 1C (true C-rate) is displayed. The capacity retention after 500 cycles is 40%. Thus, the tested structural battery cell shows poor capacity retention at this fairly high charge rate and cannot match long-term performance of the first-generation cells.[5] However, it is important to note that despite the low capacity retention, the battery maintains a high Coulombic efficiency, indicating efficient energy conversion and delivery. This implies that the battery effectively converts and delivers energy while experiencing a decline in overall capacity over time. The observed combination of low capacity
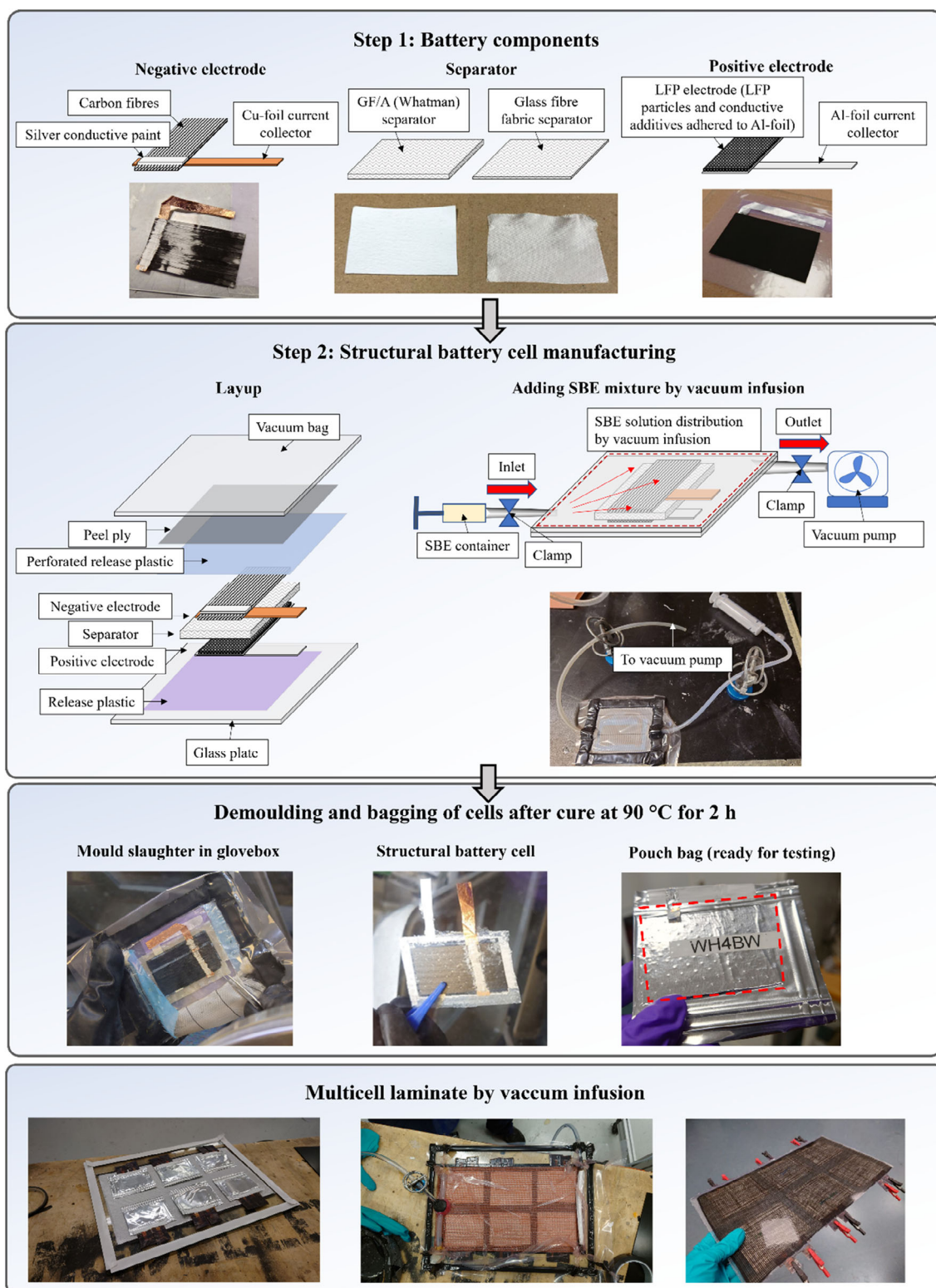
Figure 1. Structural battery composite fabrication, showing the steps: battery component manufacture; cell manufacture and curing; demulding and pouch-bagging of the structural battery composite cell; and multicell manufacture.

**ADVANCED
SCIENCE NEWS**

www.advancedsciencenews.com

**ADVANCED
ENERGY & SUSTAINABILITY
RESEARCH**
Open Access

www.advenergysustres.com

Table 1. Representative specific capacities and energy densities of the tested structural battery cells at 0.05C (i.e., a discharge time of approximately 20 h), with a nominal voltage during discharge of 2.7 V. Specific power at 1C with a nominal voltage during discharge of 2.6 V. Note that specific power reported by Asp et al. is at 3C.[5] All reported values are relative the total cell mass (i.e., accounting for all constituents).

Separator	Whatman GF/A		GF plain weave	
	Current study	Ref. [5]	Current study	Ref. [5]
Specific capacity [Ah kg^{-1}]	9.82	4.13	14.7	8.55
Energy density [Wh kg^{-1}]	25.9	11.6	41.2	23.6
Specific power [W kg^{-1}]	8.5	5.94	12.4	9.56
Total mass of cell [g cm^{-2}]	0.062	0.074	0.042	0.046
Cell thickness [mm]	0.27	0.40	0.15	0.27

retention and high Coulombic efficiency may be attributed to factors such as electrode degradation, electrolyte decomposition, or other aging mechanisms that result in reduced availability of active materials or increased internal resistance within the battery. Considering that the electrodes used in structural batteries are similar to those of conventional batteries, the main reasons for low capacity retention in structural batteries can be attributed to the SBE and its impact on ionic conductivity. The combination of salts in the SBE exhibits a lower conductivity compared to conventional Li-ion battery salts like LiPF$_6$ and LiTFSI. Additionally, the SBE's unique morphology, where the electrolyte is confined to the polymer percolating pores, directly affects the ionic conductivity.[20] This restricted distribution of liquid electrolyte limits the available pathways for ion transport and hinders the connectivity between the electrode materials. Consequently, the confinement of the liquid electrolyte within small compartments in the porous structure creates localized regions with lower ion mobility, leading to an overall decrease in ionic conductivity.

Figure 2c shows the energy density versus the true C-rate for both cells with Whatman GF/A and GF plain weave separator. In the graph, also results for first-generation cells with the two separator alternatives are plotted for comparison. Cells from the current study, manufactured by resin infusion under mild vacuum, demonstrate significantly higher energy densities at all C-rates compared to the first-generation cells.[5] Furthermore, the energy density of the structural battery cell with the GF plain weave separator is significantly higher than that of the cells with the thicker Whatman GF/A separator. Finally, in Figure 2d, Nyquist plots for the six Whatman GF/A separator cells used in the multicell demonstrator are presented. The impedance results for the individual cells show a conspicuous difference in cell resistivity between cells. Comparing electrochemical impedance spectroscopy (EIS) outcomes of the current cells manufactured by vacuum infusion with previous EIS measurements on first-generation cells reveals several notable improvements.[9] Primarily, the stark contrast in Ohmic resistance values between the first-generation cells and the current cells suggests substantial variations in the internal resistance attributable solely to the manufacturing process, as the electrode materials and electrolyte remain the same. These differences can be ascribed to various factors arising from the manufacturing process. Variances in electrode preparation results in different qualities of the electrode–electrolyte interface
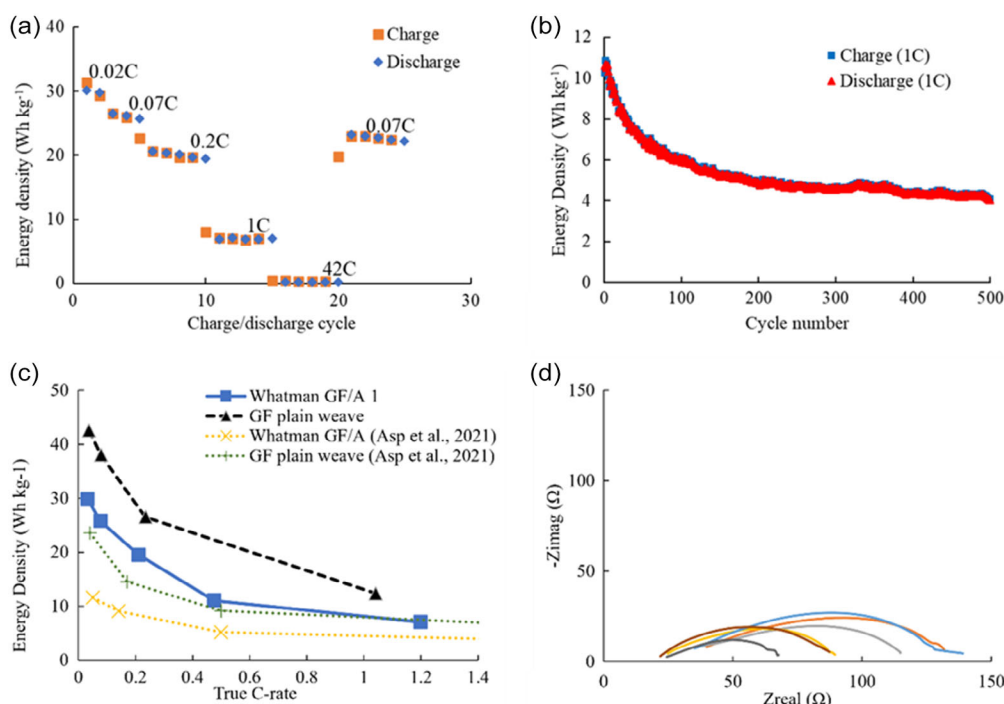

Figure 2. Results from electrochemical characterization of cells with the Whatman GF/A separator. Specific capacity and energy density are based on the mass of the battery cell. a) Energy density at different true C-rates. b) Long-term cycling at 1C. c) Energy density versus true C-rate for the two cell types and the cells from earlier work. d) Electrochemical impedance spectroscopy (EIS) measurements on the six individual cells used in the multicell demonstrator.

for both the positive and negative electrodes, consequently impacting the Ohmic resistance. Additionally, the vacuum-infusion technique enables more consistent fiber alignment and compaction, which affect the pathway and ease of ion flow, resulting in reduced resistance. The use of vacuum pressure overcomes inconsistent or incomplete wetting of the electrolyte into the negative electrode in the first-generation cells, ensuring proper impregnation of the surrounding SBE material. Furthermore, variations in separator thickness arising from the manufacturing process influence ion transport, with higher compaction levels leading to lower Ohmic resistance.

Second, the charge-transfer resistance of the resin infused cells is only approximately 20% of that of the first-generation cells as characterized by Xu et al.[9] As charge-transfer resistance relates to the kinetics of electrochemical reactions occurring at the electrode–electrolyte interface, this remarkable reduction in charge-transfer resistance can be attributed to the improved manufacturing process employed. The refined manufacturing techniques result in electrodes with smoother surfaces, free from defects, and uniform distribution of active materials. These advancements facilitate enhanced contact with the electrolyte, mitigate diffusion limitations, and promote more efficient charge transfer at the electrode–electrolyte interface.

Risk assessment of the structural battery indicates several factors that contribute to its inherent safety.[8] First, the energy density of the cell is lower than for conventional Li-ion batteries. Second, the use of carbon fiber and LFP electrode materials, similar to graphite and LFP, known for their stability and low reactivity, reduces the risk of thermal runaway. From a flammability standpoint, having smaller amounts of electrolyte in small compartments within a porous polymer structure in the SBE is generally considered safer compared to a larger volume of electrolyte in a conventional battery. The reduced fuel source provided by smaller amounts of electrolyte limits the availability of flammable material in case of a fire or thermal event. The porous polymer structure enhances heat dissipation and provides better thermal management, reducing the risk of thermal runaway. Additionally, the increased surface area-to-volume ratio of the porous structure aids in faster cooling and heat dispersion. No tests related to battery safety are performed here. Such tests are considered for future study.

For the structural battery demonstrator laminate, 14 structural battery cells with a Whatman GF/A separator were successfully manufactured. Out of these, only one cell did not work (i.e., a 7% rejection rate). This demonstrates the robustness of the employed manufacture procedure. The six highest performing cells were selected for the structural battery multicell demonstrator laminate. These cells had an average energy density of $25.9(\pm1.2)$ Wh kg^{-1}. For the galvanostatic test of the fully charged battery pack, the cells were connected in parallel (1s6p) and discharged at 9.6 mA, expecting a discharge time of 2 h. Capacity, energy, and power were calculated considering the actual recorded current, voltage, and discharge time. Similarly, a configuration with two sets of three cells in parallel connected in series (2s3p) was also tested. The results from these tests are presented in **Table 2**. Notably, the experimentally recorded discharge time for the battery pack was approximately 3 h, compared to the estimated 2 h. The improvement in cell performance repeatability allows for multicell demonstration

Table 2. Structural battery demonstrator laminate pack electrical performance for different configurations (1s6p all cells in parallel, and 2s3p two sets of three cells in parallel connected in series).

Configuration	Current [mA]	Nom. voltage [V]	Capacity [Ah]	Energy [Wh]	Power [W]	Runtime [h]
1s6p	9.6	2.86	0.029	0.084	0.027	3.05
2s3p	4.8	5.78	0.013	0.074	0.028	2.67

without need for an advanced battery management system (BMS). However, it should be noted that implementing a BMS would extend the runtime beyond what is displayed in Table 2. By employing a BMS and balancing the cells, it becomes possible to equalize the voltage across individual cells within the battery pack, resulting in enhanced overall performance. Based on the EIS measurements, which revealed only minor imbalances, it is inferred that passive balancing without additional control electronics may be sufficient. This approach involves the use of resistors to dissipate excess energy when a cell reaches its desired voltage level, allowing the cell to discharge and equalize its state of charge with the other cells.

2.2. Mechanical Performance

The mechanical properties of the structural battery composites were characterized under tensile loading. The average elastic moduli and the tensile strengths of the laminated full cells tested in in x- and y-directions, as defined in **Figure 3**, are presented in **Table 3**. In the table, mechanical properties of the first-generation cells are included for comparison.

Due to the size and thickness of the laminate, measuring mechanical properties presents certain limitations, especially in the direction perpendicular to the fibers in the negative electrode. As the micro tester used for mechanical characterization, a Deben 2 kN tensile stage, limits the length span of the specimen to maximum 20 mm, difficulties arise during preparation of slender specimens. During the preparation of the 3 mm wide specimens, debonding between the LFP coating material and the aluminum current collector occurred for the cells with Whatman GF/A separator, in both x- and y-directions. Hence, the laminates with Whatman GF/A separator were tested in the x-direction without the aluminium layer. Moreover, this debonding in the positive electrode made testing in the y-direction impossible, due to the lack of the aluminum foil, which has a role of support.

Mechanical tests were performed on structural battery cells after electrochemical cycling. In **Figure 4**, representative stress–strain curves for all specimen types and loading directions are presented.

The highest modulus, E_x, is found for the GF 0°/90° plain weave separator structural battery composite, which is expected as the continuous glass fibers in the separators (extending in the 0°-direction) are aligned with the load direction. The modulus in the y-direction, E_y, could only be obtained for the structural battery with GF 0°/90° plain weave separator. The considerably lower modulus is explained by the matrix-dominated response of the composite to tensile loads in the y-direction.
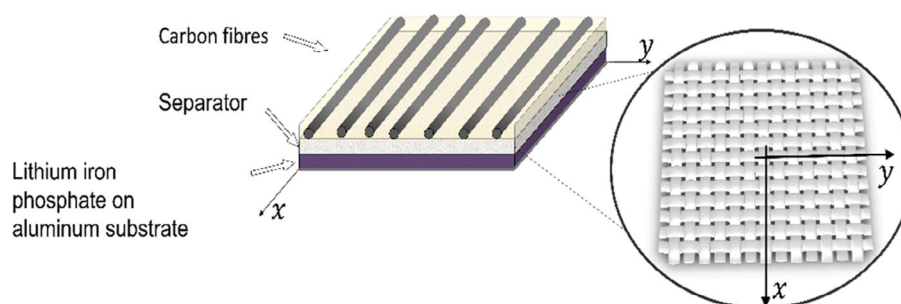
**ADVANCED
SCIENCE NEWS**

www.advancedsciencenews.com

**ADVANCED
ENERGY & SUSTAINABILITY
RESEARCH**
Open Access

www.advenergysustres.com

Figure 3. Schematics of the structural battery orientation relative to the x- and y-loading directions, and orientation of GF plain weave separator fabric.

Table 3. Mechanical properties from tensile tests of the structural battery laminates. The elastic moduli in the x- and y-directions, E_x and E_y, and the tensile strengths in the x- and y-directions, X and Y, are measured when applicable. Reported strength values are considered lower bounds as described in the experimental section.

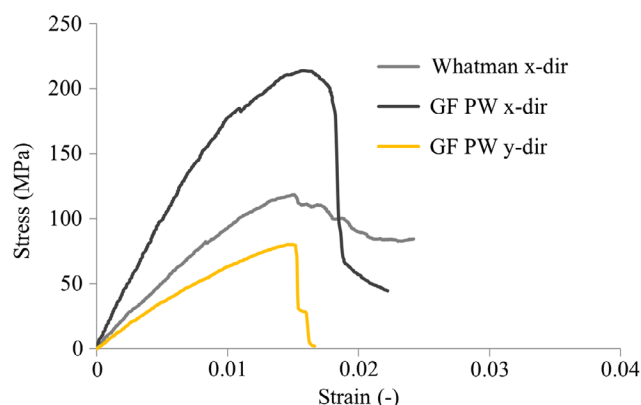| Separator	Whatman GF/A		GF plain weave 0°/90°	
	Current study	Ref. [5]	Current study	Ref. [5]
E_x [GPa]	11.5 (±0.9)	18.3 (±0.9)	25.7 (±0.09)	25.4 (±3.3)
E_y [GPa]	–	2.9 (±0.5)	8.2 (±0.7)	13.3 (±0.7)
X [MPa]	>118	>163	>213	>287
Y [MPa]	–	>16	>79	>72

Figure 4. Representative stress–strain curves from tensile tests with loading in x- and y-directions, respectively.

The relatively low scatter in measured moduli indicates that the manufacturing technique has improved significantly in terms of fiber volume fraction and fiber alignment in the negative electrode compared to previous work by Asp et al.[5]

For accurate measurements of the structural battery strength, comprehensive sample preparations including polishing free edges and tabbing clamping regions as a precaution to prevent premature failures are required. Such sample preparation was not possible, why the strength values reported in Table 2 should be regarded as lower bounds of strength of the tested materials, as most of the specimens failed in the vicinity of the grips.

The structural battery composite with GF plain weave separator had the highest recorded strength exceeding 213 MPa.

2.3. Multifunctional Performance

The multifunctional performance of the structural battery composites manufactured via resin infusion is significantly improved compared with that of the first-generation structural battery composite presented by Asp et al.[5] The improvement in multifunctional properties was caused by an improvement in electrochemical properties and no significant improvement in mechanical properties was observed. The elastic modulus and strength of the GF plain weave separator cells were maintained, whereas inconclusive results were obtained for the Whatman GF/A cells due to delamination of the cathode foil. The energy density of the cells with a GF plain weave separator was increased to 41.2 Wh kg^{-1}. This is an increase by 75% compared to the that of the first-generation cells, presented by Asp et al.[5] An even greater increase in energy density between the generations of cells was found for the Whatman GF/A separator cells. For these cells, the energy density increased from 11.6 to 27.5 Wh kg^{-1}, demonstrating a 137% increase. In summary, the best working cell type, the GF plain weave separator cell, demonstrated a multifunctional performance of 41.2 Wh kg^{-1} in energy density and 25.7 GPa in elastic modulus.

3. Conclusion

Structural battery composite materials, exploiting multifunctional constituents, have been realized and demonstrate an energy density of 41 Wh g^{-1} and an elastic modulus of 26 GPa. This corresponds to a doubling of the multifunctional performance of the structural battery composite compared with that of the first-generation structural battery. This improvement has been achieved solely by employing a repeatable manufacturing scheme, using resin infusion resembling that used for conventional composites. In addition, the manufacture process is also found to produce cells with remarkably reduced impedance. In particular, the charge-transfer resistance of the structural battery cells manufactured with the proposed resin-infusion technique is only approximately 20% of that of the first-generation cells. Consequently, the proposed manufacture process provides an important contribution toward high energy, high power, and structural battery composites for use in multicell devices.

**ADVANCED
SCIENCE NEWS**

www.advancedsciencenews.com

**ADVANCED
ENERGY & SUSTAINABILITY
RESEARCH**
Open Access

www.advenergysustres.com

4. Experimental Section

Materials: The structural battery composite cells were made from the following materials. A 14 mm wide TeXtreme unidirectional carbon fiber spread tow was used as the negative electrode. The ultrathin spread tow UD tapes of T800SC-12 k-5 °C PAN-based carbon fibers with a linear tow weight of 0.52 g m^{-1} were supplied by Oxeon AB, Sweden. The multifunctional properties of the T800S fiber were reported by, e.g., Kjell et al.[21] and Fredi et al.[22] A battery grade single side LiFePO$_4$ (LFP)-coated aluminum foil (82 μm thick; rated capacity of 1 mAh cm^{-2}) purchased from Custom Cells Itzehoe GmbH, Germany, was used as the positive electrode. Two types of glass fiber separators were used: 1) Whatman glass microfiber separator (Whatman GF/A, 260 μm thick) supplied by Sigma Aldrich; and 2) three layers of a 0°/90° woven glass fiber plain weave fabric, with a fabric surface weight of 25 g m^{-2} from R&G Faserverbundwerkstoffe, Waldenbuch, Germany. The total separator thickness of the stacked plain weave fabric layers was approximately 65 μm. The bi-continuous SBE includes the following constituents: for the polymer material part, bisphenol A ethoxylate dimethacrylate (M_n: 540 g mol^{-1}) supplied by Sartomer Europe was used; for the liquid electrolyte part, propylene carbonate (PC) (PC ≥ 99%, acid <10 ppm, H$_2$O <10 ppm) and ethylene carbonate (EC) (99% anhydrous) supplied by Sigma–Aldrich were used. Furthermore, for the SBE lithium trifluoromethanesulfonate (LiTf) (99.99%), lithium bis(oxalato)borate (LiBoB) and 2,2′-azobis(2-methylpropionitrile) (AIBN) purchased from Sigma–Aldrich were used. The multicell demonstrator laminate was made from the following materials: two electrically insulating 0°/90° glass fiber plain weaves with areal weights of 90 and 400 g m^{-2}, respectively, were used as in the structural casing. In addition, a Bcomp ampliTex 200 g m^{-2} 0°/90° low twist flax fiber weave was used. An infusion resin from Rampf Group, Grafenberg, Germany, RAMPF EI-2500 epoxy with RAMPF EH-2970-1 hardener, was used as matrix material in the demonstrator laminate. All materials were used as received.

Structural Battery Full Cell Manufacture: Cell manufacturing involved preparation of the SBE, assembly of cell components, vacuum infusion of SBE into the stacked and vacuum bagged cell, curing, followed by demolding, and sealing of the cured cell in a pouch bag. A schematic illustration of the structural battery composite full cells manufacture procedures is provided in Figure 1. Preparation of the SBE was carried out in an inert and dry environment (inside the glove box at conditions less than 1 ppm O$_2$ and 1 ppm H$_2$O) and concerned mixing of liquid electrolyte, monomer, lithium salt, and initiator. The SBE mixture was prepared in accordance with the procedure described in Schneider et al.,[14] with the only differences being that dimethyl methylphosphonate (DMMP) in the electrolyte was replaced with PC. The SBE solution was made by mixing 50:50 wt% of 1) a liquid electrolyte solution made from the mixture of LiBoB and LiTf at concentrations of 0.4 and 0.6 M, respectively, in EC:PC 1:1 w/w (50:50 wt%); and 2) monomer bisphenol A ethoxylate dimethacrylate and the thermal initiator, AIBN (1 wt% of the monomer weight). The SBE mixture was stirred into a homogenous solution using a vortex. After mixing, the SBE samples were degassed at a low pressure (−0.2 bar Δ pressure) to remove any gas bubbles from the solution. For this purpose, the sample container lid was replaced with a perforated lid and the sample was placed inside the transfer chamber of the glove box where the pressure could be controlled in an argon environment. The solution was degassed for 3 min. The sample was then brought back into the glove box and transferred into a syringe, allowing it to be connected to the infusion setup outside the glove box.

Cell components were sized and assembled on a glass plate which was also used as the mold for the cells. Negative electrodes were prepared by placing carbon fiber (CF) spread tows on a separate glass plate with copper current collectors placed underneath and then bonded to the fibers using a conductive silver paint before cut into size. Positive electrodes were prepared by cutting LFP-coated foils to match the size of the CF electrodes. The electrodes were 28 mm wide and 50 mm long, with the length extending along the carbon fibers in the UD spread tow. This corresponded to approximately 59 mg of carbon fibers and 118 mg of LFP particles in the complete structural battery cell. Aluminum current collectors were fixed on back (Al side) of the cathode foils and folded around the edge for a more reliable anchor. Plain release plastics were used on the glass

plates (instead of any release chemicals to avoid contaminations) over which the components were positioned. First, the LFP foil was placed with the Al collector foil facing the glass plate. Second, a separator (4 cm × 6 cm) was placed on top of the positive electrode and finally the CF electrode was stacked on top and aligned with visual accuracy. Placement of the positive and negative electrodes was very important for consistent performance of the manufactured cells. The CF electrodes required extra inspection because of any loose fibers could cause the cell to short circuit. The assembled cell components were then covered with perforated release plastic and a peel ply. The cell assembly was vacuum bagged and dried in an oven at 50 °C 14 h inside a desiccator. All vacuum bagged dry cell assembly had 4 mm silicone tubes as inlet and outlet with clamps. This simple system can be sealed using the clamps on both sides once the syringe with SBE was integrated. Infusion was carried out at a pressure of −0.5 bar. Pressure was regulated using a vacuum valve. Once the pressure was set, clamps were opened (outlet first) slowly to start the infusion process. At the end of infusion, clamps were closed (inlet first), the system was detached from the pump and left in an oven for curing at 90 °C for 2 h. A video showing the infusion setup is provided as part of Supporting Information. Cured cells were taken inside the glove box, demolded, and sealed in a pouch bag (polyethylene terephthalate (PET):aluminium (Al):polyethylene (PE), 12 μm:9 μm:75 μm thickness) or carefully cut into slender pieces for mechanical testing. Cross sections of the two types of cells, with Whatman GF/A and GF plain weave separator fabrics, are presented in Figure S2, Supporting Information.

In total, 23 structural battery composite cells were manufactured and characterized for their multifunctional performance. Among these, 20 were made using a Whatman GF/A separator and 3 with the GF plain weave separator.

Electrochemical Testing: The structural battery cells were preconditioned by galvanostatic cycling at a constant current of 0.300 mA for 10 complete charge/discharge cycles. Galvanostatic charge and discharge (GCD) cycling was continued at 0.567 mA for 5 cycles and the resulting specific capacity and energy density were calculated. All of these tests were done using Neware CT-4008-5V10mA-164 battery cycler. The cells were cycled between 2.00 and 3.55 V using a series of current densities or C-rates. The selected current for the charge/discharge cycles was based on the theoretical C-rate calculated from the area capacity of the LFP-positive electrode, which was 1 mAh cm^{-2}. For testing the long-term performance of the structural battery composite, one cell was exposed to a long-term cycling exceeding 500 cycles of GCD at a rate of 1 C. Moreover, electrochemical characterization was performed at different C-rates for each cell type, i.e., for the two different separator solutions. The cells were cycled at the following theoretical rates: 0.025C, 0.05C, 0.1C, 0.2C, and 0.4C. Between each charge and discharge cycle, a resting time of 60 min was used to allow ion-concentration gradients to relax. Finally, EIS was performed on the individual cells. These tests were performed to measure the impedance of the structural battery cells. EIS measurements were performed in the frequency range from 200 kHz to 1 Hz under an alternating current (AC).

Mechanical Testing: Tensile tests were carried out to characterize the elastic properties of the laminate in *x*- and *y*-directions, as defined in Figure 3. The mechanical tests followed procedures developed by Asp et al.[5] Due to the dimensions of the full cell, measuring mechanical properties of the structural battery composite presented certain limitations. For these, specimen conventional techniques such as digital image correlation or strain gauges could not be used to measure strain. The micro tester used for mechanical characterization, a Deben 2 kN tensile stage, further prevented use of conventional test standards, such as ASTM D3039. For this reason, test specimen dimensions were adjusted to fit the test equipment.

Mechanical tests were performed on structural battery cells after electrochemical cycling. Consequently, the tensile tests were performed inside a glove box (in inert and dry conditions, less than 1 ppm O$_2$ and 1 ppm H$_2$O). A photo showing the mechanical test setup inside the glove box is presented in Figure S3, Supporting information. No tests were performed on pristine structural battery cells. Slender test specimens, 30 mm in length and 3.0 mm in width, were cut from the GCD cycled structural battery cells with great caution to allow for precise measure of the elastic modulus. Accurate measurement of composite strength, however,

required comprehensive sample preparation, involving polishing free edges and tabbing clamping regions to prevent premature failure, and hence underestimated material strength. Such sample preparations were not possible here. Tensile tests were made on a minimum of five samples per specimen type. Tensile tests were performed under displacement control at a rate of 0.2 mm min^{-1}. Applied strain used to determine the moduli was calculated from the crosshead displacement of the micro tester, and the machine compliance was compensated following compliance calibration procedures described in ASTM D3379 and Asp et al.[5] This procedure allowed for precise determination of the true compliance by deducting the machine compliance from the apparent compliance. As a result, the moduli could be accurately calculated.

Multicell Demonstrator Manufacture and Electrochemical Characterization: A multicell demonstrator using six cells was manufactured at Volvo Cars' Concept Center. Individual cells were arranged and enclosed in several electrically insulating layers of composite materials to form a single laminate (structural battery demonstrator laminate). The manufactured multicell structural battery demonstrator laminate is depicted in Figure 1, and a Schematic diagram of the layers applied for the laminate can be found in Figure S4, Supporting Information. The layups were vacuum infused at −1 bar with the epoxy-hardener mix (10:3 respective mass ratio) and cured initially at room temperature overnight and then post-cured at 50 °C for 8 h. The laminate had individual connection points for the cells allowing them to be connected externally in any desired configuration, as illustrated in Figure S5, Supporting Information. Current collectors from the cells were taped with release plastic caps to avoid contact with electrically conductive surrounding materials. As a result, the cells could be charged separately and discharged in a configured circuit, eliminating the need of a BMS. The structural battery demonstrator laminate was connected and tested electrochemically in two configurations. In the first configuration, the six cells were connected in parallel (1s6p), and in the second, two sets of three cells in parallel (2s3p) were connected in series. The GCD tests were carried out at 9.6 mA (1.6 mA × 6) for the 1s6p configuration and at 4.8 mA for the 2s3p arrangement. The current levels were estimated based on an expected discharge time of 2 h.

Supporting Information

Supporting Information is available from the Wiley Online Library or from the author.

Conflict of Interest

The authors declare no conflict of interest.

Data Availability Statement

The data that support the findings of this study are available from the corresponding author upon reasonable request.

[1] *European Green Deal: Commission Proposes Transformation of EU Economy and Society to Meet Climate Ambitions*, European Commission, July **2021**.

[2] D. Carlstedt, L. E. Asp, *Composites, Part B* **2020**, *186*, 107822.

[3] A. Lendlein, R. S. Trask, *Multifunct. Mater.* **2018**, *1*, 010201.

[4] A. Ishfaq, S. N. Nguyen, E. S. Greenhalgh, M. S. P. Shaffer, A. R. J. Kucernak, L. E. Asp, D. Zenkert, P. Linde, *J. Compos. Mater.* **2023**, *57*, 817.

[5] L. E. Asp, K. Bouton, D. Carlstedt, S. Duan, R. Harnden, W. Johannisson, M. Johansen, M. Johansson, G. Lindbergh, F. Liu, K. Peuvot, L. M. Schneider, J. Xu, D. Zenkert, *Adv. Energy Sustainability Res.* **2021**, *2*, 2000093.

[6] G. J. H. Lim, K. K. Chan, N. A. A. Sutrisnoh, M. Srinivasan, *Mater. Today Sustainability* **2022**, *20*, 100252.

[7] T. Jin, G. Singer, K. Liang, Y. Yuan, *Mater. Today* **2023**, *62*, 151.

[8] S. Kalnaus, L. E. Asp, J. Li, G. M. Veith, J. Nanda, C. Daniel, X. C. Chen, A. Westover, N. J. Dudney, *J. Energy Storage* **2021**, *40*, 102747.

[9] J. Xu, Z. Geng, M. Johansen, D. Carlstedt, S. Duan, T. Thiringer, F. Liu, L. E. Asp, *EcoMat* **2022**, e12180.

[10] L. E. Asp, M. Johansson, G. Lindbergh, J. Xu, D. Zenkert, *Funct. Compos. Struct.* **2019**, *1*, 042001.

[11] J. Hagberg, H. A. Maples, K. S. P. Alvim, J. Xu, W. Johannisson, A. Bismarck, D. Zenkert, G. Lindbergh, *Compos. Sci. Technol.* **2018**, *162*, 235.

[12] J. S. Sanchez, J. Xu, Z. Xia, J. Sun, L. E. Asp, V. Palermo, *Compos. Sci. Technol.* **2021**, *208*, 108768.

[13] N. Ihrner, W. Johannisson, F. Sieland, D. Zenkert, M. Johansson, *J. Mater. Chem. A* **2017**, *5*, 25652.

[14] L. Schneider, N. Ihrner, D. Zenkert, M. Johansson, *ACS Appl. Energy Mater.* **2019**, *2*, 4362.

[15] V. Tu, L. E. Asp, N. Shirshova, F. Larsson, K. Runesson, R. Jänicke, *Multifunct. Mater.* **2020**, *3*, 025001.

[16] W. Johannisson, N. Ihrner, D. Zenkert, M. Johansson, D. Carlstedt, L. E. Asp, F. Sieland, *Compos. Sci. Technol.* **2018**, *168*, 81.

[17] W. Johannisson, R. Harnden, D. Zenkert, G. Lindbergh, *Proc. Natl. Acad. Sci. U.S.A.* **2020**, *117*, 7658.

[18] R. Harnden, D. Carlstedt, D. Zenkert, G. Lindbergh, *ACS Appl. Mater. Interfaces* **2022**, *14*, 33871.

[19] E. S. Greenhalgh, S. Nguyen, M. Valkova, N. Shirshova, M. S. P. Shaffer, A. R. J. Kucernak, *Compos. Sci. Technol.* **2023**, *235*, 109968.

[20] S. Duan, M. Cattaruzza, V. Tu, R. M. Auenhammer, R. Jänicke, M. K. G. Johansson, F. Liu, L. E. Asp. *Commun. Mater.* **2023**, *4*, 49.

[21] M. H. Kjell, E. Jacques, D. Zenkert, M. Behm, G. Lindbergh, *J. Electrochem. Soc.* **2011**, *158*, A1455.

[22] G. Fredi, S. Jeschke, A. Boulaoued, J. Wallenstein, M. Rashidi, F. Liu, R. Harnden, D. Zenkert, J. Hagberg, G. Lindbergh, P. Johansson, L. Stievano, L. E. Asp, *Multifunct. Mater.* **2018**, *1*, 015003.